AGU PUBLICATIONS

Water Resources Research

RESEARCH ARTICLE
10.1002/2016WR020234

Key Points:
- First application of monitoring a mountain snowpack via cosmic-ray neutron sensing (CRNS)
- High correlation with both snow depth and water equivalent obtained via Terrestrial Laser Scanning (TLS)
- No complete saturation of CRNS signal even for snowpacks up to 600 mm snow water equivalent

Supporting Information:
- Supporting Information S1

Correspondence to:
P. Schattan,
schattan@alps-gmbh.com

Citation:
Schattan, P., G. Baroni, S. E. Oswald, J. Schöber, C. Fey, C. Kormann, M. Huttenlau, and S. Achleitner (2017), Continuous monitoring of snowpack dynamics in alpine terrain by aboveground neutron sensing, *Water Resour. Res.*, *53*, 3615–3634, doi:10.1002/2016WR020234.

Received 7 DEC 2016
Accepted 5 APR 2017
Accepted article online 11 APR 2017
Published online 2 MAY 2017

Continuous monitoring of snowpack dynamics in alpine terrain by aboveground neutron sensing

Paul Schattan[1,2], Gabriele Baroni[3,4], Sascha E. Oswald[4], Johannes Schöber[5], Christine Fey[1,5], Christoph Kormann[4], Matthias Huttenlau[1], and Stefan Achleitner[6]

[1]alpS Centre for Climate Change Adaptation, Innsbruck, Austria, [2]Institute of Geography, University of Innsbruck, Innsbruck, Austria, [3]Subsurface Hydrology Group, Department of Computational Hydrosystems, UFZ–Helmholtz Centre for Environmental Research, Leipzig, Germany, [4]Institute of Earth and Environmental Science, University of Potsdam, Potsdam, Germany, [5]TIWAG Tiroler Wasserkraft AG, Innsbruck, Austria, [6]Unit of Hydraulic Engineering, University of Innsbruck, Innsbruck, Austria

Abstract The characteristics of an aboveground cosmic-ray neutron sensor (CRNS) are evaluated for monitoring a mountain snowpack in the Austrian Alps from March 2014 to June 2016. Neutron counts were compared to continuous point-scale snow depth (SD) and snow-water-equivalent (SWE) measurements from an automatic weather station with a maximum SWE of 600 mm (April 2014). Several spatially distributed Terrestrial Laser Scanning (TLS)-based SD and SWE maps were additionally used. A strong nonlinear correlation is found for both SD and SWE. The representative footprint of the CRNS is in the range of 230–270 m. In contrast to previous studies suggesting signal saturation at around 100 mm of SWE, no complete signal saturation was observed. These results imply that CRNS could be transferred into an unprecedented method for continuous detection of spatially averaged SD and SWE for alpine snowpacks, though with sensitivity decreasing with increasing SWE. While initially different functions were found for accumulation and melting season conditions, this could be resolved by accounting for a limited measurement depth. This depth limit is in the range of 200 mm of SWE for dense snowpacks with high liquid water contents and associated snow density values around 450 kg m^{-3} and above. In contrast to prior studies with shallow snowpacks, interannual transferability of the results is very high regardless of presnowfall soil moisture conditions. This underlines the unexpectedly high potential of CRNS to close the gap between point-scale measurements, hydrological models, and remote sensing of the cryosphere in alpine terrain.

1. Introduction

Mountain regions are considered as the "water towers" of the surrounding low lands [*Liniger et al.*, 1998; *Viviroli et al.*, 2007] with snow melt often being of major importance for its fresh water supply [*Sturm*, 2015]. Snow state data from both ground-based measurements and remote sensing products are increasingly used for snow hydrological applications including multiobjective calibration of hydrological models [*Kirnbauer et al.*, 1994; *Finger et al.*, 2011, 2015; *Schöber et al.*, 2014; *Berezowski et al.*, 2015; *Revuelto et al.*, 2016], reverse modeling of basin-scale precipitation [*Shrestha et al.*, 2014; *Henn et al.*, 2016], and data assimilation [*Slater and Clark*, 2006; *Thirel et al.*, 2013; *Magnusson et al.*, 2014].

Measurements of environmental variables can be classified by (i) their support, i.e., the integration volume of the signal detected, (ii) the spatial spacing between two measurements, (iii) the extent of the totally measured area, and (iv) the repeat frequency [*Blöschl and Sivapalan*, 1995; *Sturm*, 2015]. Mountain snowpacks are characterized by complex layering and a high variability in time and space [*Sturm et al.*, 1995]. Therefore, measurements of snow state variables in mountain areas ideally combine a support of intermediate spatial scale of several hectares, a small spacing, an extent of the entire basin and a high repeat frequency. Other aspects to be considered include (i) low disturbances of both the snowpack itself and the snow accumulation patterns, (ii) the applicability in a wide range of terrain and snowpack properties, and (iii) acceptable costs for installation and maintenance [*Lundberg et al.*, 2010].

Traditional snow sampling techniques (snow pits, snow core surveys) [*Goodison et al.*, 1987; *Kinar and Pomeroy*, 2015; *Proksch et al.*, 2016] are invasive, labor intensive, and suffer from several drawbacks like small support, large spacing and/or low repeat frequency. A number of automated in situ measurements for

snow depth (SD), snow water equivalent (SWE), or liquid water content exist [*Johnson and Marks*, 2004; *Stähli et al*., 2004; *Egli et al*., 2009; *Lundberg et al*., 2010; *Koch et al*., 2014] but are usually limited to a very small support with a high sensitivity to local anomalies. For widely used instruments like snow pillows or snow scales, other issues include disturbances of the snowpack due to energy transport into the snowpack, changes of the wind field, or a high sensitivity to varying snow properties, such as changes in snow density or the development of thin ice layers [*Johnson and Marks*, 2004; *Lundberg et al*., 2010].

Space-borne remote sensing products would overcome these limitations and meet most of the requirements presented before. But unlike snow-covered area, which has been operationally monitored using optical satellite data for decades [*Dozier*, 1989; *Hall et al*., 1995, 2002; *Nolin*, 2010; *Dietz et al*., 2012; *Frei et al*., 2012; *Rittger et al*., 2013], monitoring other snow properties in mountain areas remains challenging [*Lundberg et al*., 2010; *Nolin*, 2010; *Kinar and Pomeroy*, 2015; *Sturm*, 2015; *Lundberg et al*., 2016]. In satellite-based SWE products, mountain ranges are masked out due to the low sensor resolution of several kilometers [*Rott et al*., 2004; *Liang et al*., 2008; *Clifford*, 2010; *Nolin*, 2010; *Dietz et al*., 2012]. Recent developments based on high-resolution Synthetic Aperture Radar satellites allow for mapping wet snow cover [*Rott et al*., 2004, 2012; *Pettinato et al*., 2013; *Nagler et al*., 2016; *Rondeau-Genesse et al*., 2016]. However, no information related to the mass of the snowpack like SD or SWE can be retrieved. High costs and low repeat frequencies hamper the use of airborne techniques like passive gamma-ray measurements [*Peck et al*., 1971; *Lundberg et al*., 2010; *Kinar and Pomeroy*, 2015], airborne light detection and ranging (LiDAR) [*Deems et al*., 2013; *Bhardwaj et al*., 2016], or airborne photogrammetry [*Bühler et al*., 2015; *Jagt et al*., 2015; *Nolan et al*., 2015].

Recently, promising measurement techniques combining a larger support with low maintenance cost like acoustic-sounding of the snow pack [*Kinar and Pomeroy*, 2007], aboveground gamma-ray scintillators [*Choquette et al*., 2013], GPS interferometric reflectometry [*Gutmann et al*., 2012], or aboveground cosmic-ray neutron sensors (CRNS) [*Desilets et al*., 2010] have been suggested for monitoring SWE. While buried cosmic-ray neutron probes [*Kodama*, 1980; *Avdyushin et al*., 1982; *Paquet and Laval*, 2006] have a small support and potentially disturb energy fluxes into the snowpack, the aboveground CRNS technique is characterized by a support of several hectares [*Desilets et al*., 2010; *Zreda et al*., 2012; *Desilets and Zreda*, 2013; *Köhli et al*., 2015]. Originally proposed to monitor soil moisture [*Zreda et al*., 2008; *Desilets et al*., 2010] and also to infer soil parameters [*Rivera Villarreyes et al*., 2014; *Baatz et al*., 2016], CRNS has been demonstrated to be sensitive also to other hydrogen pools like biomass [*Franz et al*., 2012a; *Bogena et al*., 2013; *Baroni and Oswald*, 2015] or snow [*Desilets et al*., 2010; *Rivera Villarreyes et al*., 2011; *Rasmussen et al*., 2012; *Zweck et al*., 2013; *Sigouin and Si*, 2016]. The COSMIC operator [*Shuttleworth et al*., 2013] enables effective data assimilation for snow-free environments. As approaches to separate the signal of different hydrogen pools are emerging [*Baatz et al*., 2015; *Baroni and Oswald*, 2015; *Franz et al*., 2016; *Heidbüchel et al*., 2016; *Tian et al*., 2016], applications in other environments than open fields, including measurements of snow canopy interactions, are promising [*Desilets*, 2014].

The empirical knowledge of using CRNS for monitoring snowpacks is, however, limited to shallow snowpacks with rather uniform evolution. The range of SWE values covered in existing field studies is very limited and does not exceed 70 mm [*Rasmussen et al*., 2012; *Sigouin and Si*, 2016] to 130 mm [*Desilets et al*., 2010]. A saturation level at 100 mm is presumed with no sensitivity of CRNS remaining to additional amounts of snow above that [*Franz et al*., 2012b; *Desilets*, 2014]. Results from neutron modeling [*Zweck et al*., 2013] and field observations [*Sigouin and Si*, 2016] suggest that for shallow snow packs there is a mixed signal from soil moisture and snow. Two of the existing study sites are located in level, homogeneous terrain with a rather uniform snowpack [*Rasmussen et al*., 2012; *Sigouin and Si*, 2016]. In contrast, heterogeneity of the spatial patterns of snowpack accumulation and melt was reported to alter the neutron count rates during the melt season at the Mt. Lemmon Cosmic Ray Laboratory [*Desilets et al*., 2010]. Neutron count rates from all studies show a sharp decline in neutron count rates with the onset of snow accumulation as compared to snow-free conditions [*Desilets et al*., 2010; *Rasmussen et al*., 2012; *Delunel et al*., 2014; *Sigouin and Si*, 2016]. Not all of these studies provide a functional relationship between neutron counts and snow properties. For the test site in Saskatoon (Canada), a linear fit between neutron count rates and SWE was found sufficient [*Sigouin and Si*, 2016]. Previous applications with buried probes showed that neutron penetration into the snowpack follows an exponential function [*Kodama*, 1980; *Avdyushin et al*., 1982]. Theoretical analysis of interactions between snow and neutrons confirm this strongly nonlinear relationship [*Morris*, 2008; *Franz et al*., 2012b].

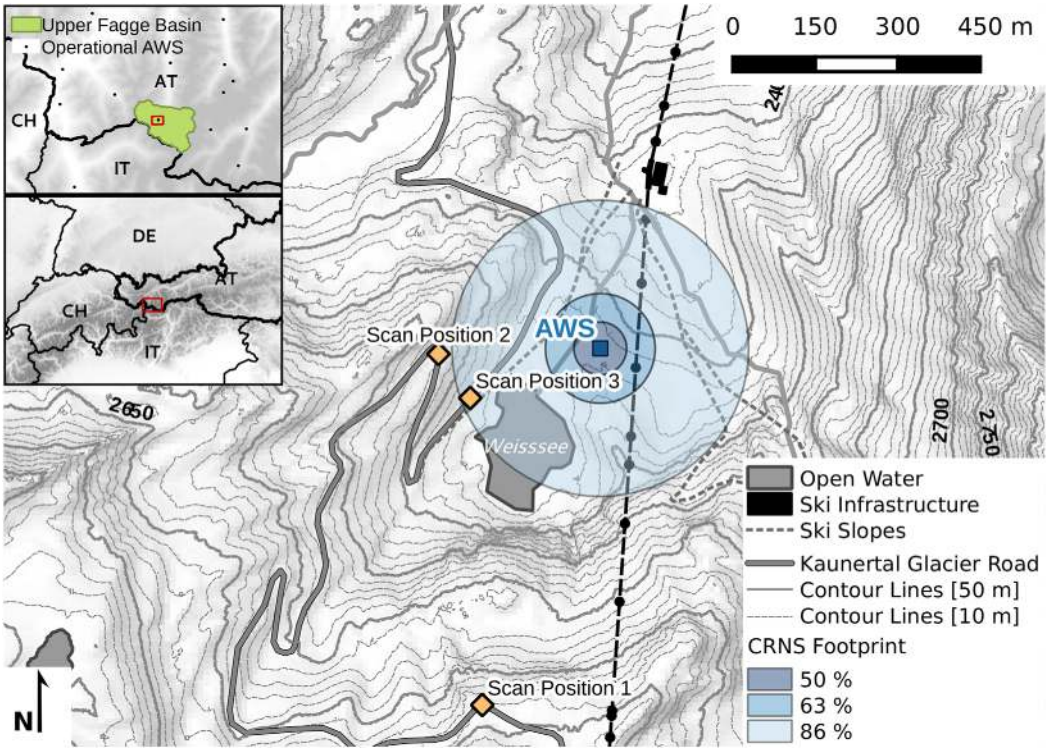

Figure 1. Study area within the Upper Fagge River (green) in the Austrian Alps. The TLS positions (yellow) are chosen to cover the theoretical footprint above snow around the Weisssee automatic weather station (AWS). The approximate CRNS footprint from where 86% of neutrons originate is marked by blue colors. The areas from where 63% and 50% of neutrons originate are marked with darker color to illustrate the spatially nonlinear nature of the footprint.

In this study, the aim was to address the following questions: (i) Does CRNS work in the extreme conditions of a high altitude site with a complex and relatively deep mountain snowpack?, (ii) Does the CRNS signal show a saturation level for the high snow depths occurring here?, (iii) Is the neutron signal sensitive to snow mass (SWE) alone or is there also an effect of the absolute thickness of the snow layer (SD)?, and (iv) Is there still a signal contribution from soil moisture when there is snow cover, and when can the signal be attributed predominantly to the snowpack?.

To investigate these issues, a field experiment in the Austrian Alps was set up to combine a CNRS measurement with point-based monitoring of the snowpack as well as special campaigns yielding a spatially highly resolved SD estimate over an area comparable to the CRNS footprint. The study period covered three winter seasons, and in 2 years the complete snow season from first snow fall to melting of the last snow cover was monitored by CRNS.

2. Experimental Site

The study area is within a gauged headwater catchment of the Fagge River, a major tributary of the Inn River in Tyrol, Austria and is located in the Ötztal Alps close to the main alpine ridge, near the border to Italy and Switzerland (Figure 1). It exhibits high precipitation amounts originating from both north-western and southern storms. An automatic weather station (AWS) is operated in vicinity of the lake Weisssee (2480 m a.s.l.). The station is equipped with standard meteorological sensors for measuring temperature, precipitation, wind speed, wind direction, and surface energy fluxes.

The AWS is surrounded by relatively level alpine terrain. The elevation ranges between 2420 and 2500 m a.s.l. within a 230 m radius around the AWS. The mean slope is 14.5 $\pm$ 10.0°. Still, SD values are highly variable due to small-scale changes in terrain roughness and surface energy fluxes (Figure 2). Snow coverage during snow accumulation is close to 100% with SD values of up to two meters at the AWS. The melting season, in contrast, is characterized by a patchy snow cover. The soils are shallow with high skeleton fractions of gravel to rocks from a glacial ground moraine and have only very little vegetation.

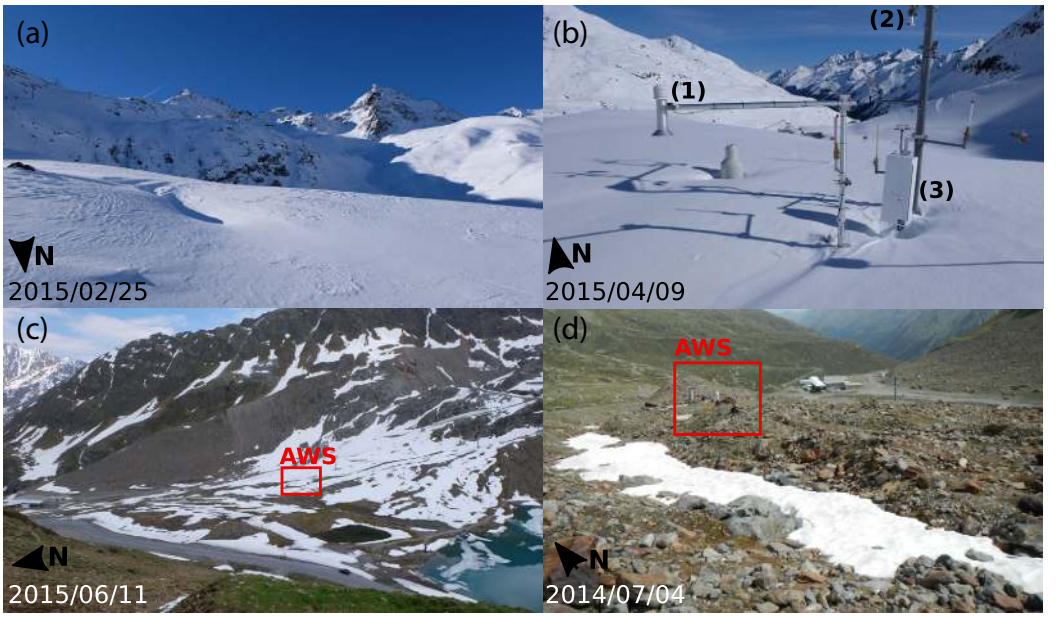

Figure 2. The test site Weisssee during the measurement season: (a) the test site next to the automated weather station (AWS), (b) the AWS in mid-winter conditions during the highest accumulation in terms of both snow depth and snow water equivalent, (c) and (d) with patchy snowpack during the melting period. The numbers (1) and (2) indicate the ultrasonic snow depth sensors. The Snow-Pack-Analyzer is located beneath sensor (1) and is almost completely buried with snow. The cosmic-ray neutron sensor (CRNS) is mounted at a height of ~2.7 m above the snow-free surface (3).

At the AWS a device for cosmic-ray neutron sensing was mounted and operated during three snow seasons to obtain neutron counts representing a spatially averaged contribution of snow and soil water. A skiing area with cable car infrastructure and two skiing slopes occupies a parts of the outer CRNS footprint. The Kaunertal glacier road with a number of viewpoints allows for all-year access to the field site facilitating Terrestrial Laser Scanning (TLS) campaigns during the winter season.

3. Data and Methods

3.1. Continuous Point-Scale Snow Measurements

Point-scale measurements are defined in general as measurements with small support in the range of maximally a few square meter and typically large spacing in the range of several meters to kilometers. In the present study, such continuous measurements of SD and snow density are processed at an hourly time step. Point-scale SD values are provided by two ultrasonic sensors (USH-8, Sommer). SD is measured based on ultrasonic distance ranging with a nominal accuracy of 0.1% but empirically being on the order of a few centimeters. While the first sensor was operated during the complete period of the field experiment, the second sensor was installed some months after the start of the study period in October 2014. Both sensors have a support of around 1 m^2 and are installed north and south of the AWS in a distance of around 2 m (Figure 2). Differences related to microscale snowpack heterogeneity of SD were observed in the order of $\pm$0.4 m between the two sensors. As the measurement infrastructure affects the local wind field, the values of both measurements are averaged to increase robustness.

Since October 2014, bulk snow density is continuously monitored by a Snow-Pack-Analyzer (Sommer) [*Stähli et al*., 2004]. Based on the different dielectric constants of ice, water, and air, bulk snow density is inferred from measurements of impedance along a diagonally installed flat ribbon sensor. Due to the setup of the Snow-Pack-Analyzer for SD values below approximately 0.5 m, the diagonal sensor is influenced by high noise, and snow density is underestimated. Additional measurements from three horizontal flat ribbon sensors (10, 30, and 50 cm above ground) are used as a substitute in this case for the automated point-scale measurements. During the first winter season, sometimes air pockets appeared around the diagonal sensor, which is a known technical problem reported also by a prior study [*Stähli et al*., 2004]. The Snow-

Pack-Analyzer was therefore reconfigured in August 2015 when the frame of the sensor was turned by about 90° to be parallel to the local wind field. For the 17 dates with snow pit measurements available (in both winter seasons), the correlation between manually and automatically observed snow density had an coefficient of determination r^2 of 0.79 and a root means squared error (RMSE) of 55 kg m^{-3} being partly caused by differing SD (RMSE = 27 cm). Observed bulk snow density ρ_{snow} in kg m^{-3} and SD in m are used to calculate SWE in mm as follows:

$$SWE = \rho_{snow} \cdot SD \quad (1)$$

3.2. Snow Measurement Campaigns

Spatially distributed measurements refer to quasi-distributed measurements consisting of a very high number of individual measurement points that have small support each but due to their dense spacing together cover large parts of the test site. During the monitoring season, 18 measurement campaigns were conducted (Table 1). Each campaign comprises of (a) spatially distributed SD measurements and (b) supporting snow pits for obtaining SD and snow density.

A first distributed SD survey was conducted using manual-scaled probe-based measurements along a north-south and an east-west transect in May 2014. For higher representativeness, three individual measurements were averaged at each of the 30 measurement points. During the following two winter seasons, a snow-free reference campaign in October 2014 and a total of 17 TLS-based snow campaigns were conducted (Table 1). Two long-range laser scanners (VZ-4000 and VZ-6000, Riegl) were used in the campaigns. Differing in laser wave length, the VZ-6000 laser scanner has a comparable performance on snow-free and dry snow surfaces but is better suited than the VZ-4000 for melting snow surfaces. The measurement accuracy is in the range of few centimeters [*Deems et al*., 2015; *Hartzell et al*., 2015]. As terrain features in the line-of-sight between the laser scanner and the surface result in data gaps, measurements were performed from three different scan positions to increase the spatial coverage (Figure 2). Due to technical reasons, six campaigns feature fewer scan positions (Table 1). Being a LiDAR-based measurement, a point cloud of surface elevation measurements is produced for each campaign. In the following step, the point cloud is aggregated to a 1 × 1 m grid. Distributed SD values are calculated by subtracting the resulting surface elevation grid from the snow-free reference elevation model (based on the campaign on 7 October 2014):

$$SD_{distribued} = DEM_{snow} - DEM_{snow\text{-}free} \quad (2)$$

Pixels with SD values smaller than 3 cm were classified as snow-free terrain. Eleven TLS campaigns during the 2014/2015 season and six campaigns during the 2015/2016 season allow for mapping within-site SD

Table 1. Snow Measurement Campaigns During the Winter Seasons 2014/2015 and 2015/2016

Survey Date	Instrument	Scan Positions	Number of Data Points (Thousands)	Number of Snow-Free Data Points (%)	Number of Snow Pits
2 May 2014	Scaled Probe		0.030	0.0	2
7 Oct 2014	Riegl VZ-4000	1, 2	130	100.0	
14 Nov 2014	Riegl VZ-6000	1, 2	124	12.6	1
19 Dec 2014	Riegl VZ-6000	1, 2, 3	107	4.8	1
13 Jan 2015	Riegl VZ-6000	1, 2, 3	120	1.9	1
12 Feb 2015	Riegl VZ-6000	1	109	3.2	1
25 Feb 2015	Riegl VZ-6000	2	86	1.9	1
18 Mar 2015	Riegl VZ-6000	1, 2, 3	125	2.7	1
9 Apr 2015	Riegl VZ-6000	1, 2, 3	126	1.5	1
17 May 2015	Riegl VZ-6000	1, 2, 3	126	9.1	1
5 Jun 2015	Riegl VZ-6000	1, 2, 3	125	23.1	1
11 Jun 2015	Riegl VZ-6000	1, 2, 3	126	52.1	1
22 Jun 2015	Riegl VZ-6000	1, 2, 3	126	92.1	3
24 Nov 2015	Riegl VZ-6000	1	106	53.2	2
3 Dec 2015	Riegl VZ-4000	1, 2, 3	120	20.6	1
4 Mar 2016	Riegl VZ-4000	1, 2	103	1.4	-
28 Apr 2016	Riegl VZ-4000	1, 2, 3	121	3.5	6
7 Jun 2016	Riegl VZ-6000	1, 2, 3	125	36.5	1
29 Jun 2016	Riegl VZ-6000	1, 2, 3	129	96.5	2

distributions at contrasting snow accumulation and melt conditions. The resulting distributed SD maps cover 86–130 thousand data points within a 230 m radius around the station. The fraction of snow-free data points ranges between 1.4% during accumulation on 4 April 2016 and 96.5% at the end of the melting season on 29 June 2016.

The coefficient of variation (CV) [*Marchand and Killingtveit*, 2005] is calculated from the standard deviation within the 230 m radius and the corresponding average SD as a measure for within-site variability of distributed SD values:

$$CV = \frac{\sigma_{SD}}{\overline{SD}} \tag{3}$$

In a snow pit near the AWS, individual layers are cut and weighted using a tube of a length of 21 cm and known volume. Bulk snow density is calculated by averaging the single measurements. SD is measured by a scaled stick with 1 cm resolution. Snow density and SD can be used to infer point-scale SWE with an accuracy of ± 10% [*Stuefer et al*., 2013].

The within-site variability of snow density is considerably lower for snow density than it is for SD [*Jonas et al*., 2009; *Sturm et al*., 2010; *López-Moreno et al*., 2013; *Schöber et al*., 2016]. Variability of SWE therefore largely follows the spatial distribution of SD [*Sturm et al*., 2010; *López-Moreno et al*., 2013]. Self-compaction is one of the main drivers for within-site variations of snow density. To verify the impact of SD on snow density at the study site and to describe its within-site variability, a total of seven measurement points were collected on 28 April 2016 within the area where 50% of neutrons originate (Figure 2). In addition to the values recorded by the AWS, this included six snow pit bulk density measurements with differing SD.

SD values of the snow pits varied between 73 and 201 cm, corresponding to a range of snow density between 323 and 411 kg m^{-3}. The resulting within-site variability of snow density in terms of CV is 8%, which is at the lower end of the values in the range of 7–32% reported by other studies [*Jonas et al*., 2009; *Sturm et al*., 2010; *López-Moreno et al*., 2013; *Schöber et al*., 2016]. This corresponds to the fact that transects reported in the literature include a larger elevation range than is found at the study site. The CV of SD values is 34%.

A snow density fraction ρ_F and a SD fraction SD_F were calculated to normalize the individual measurements in respect to the corresponding mean values of snow density and SD:

$$\rho_F = \frac{\rho_i - \overline{\rho}}{\overline{\rho}} \tag{4}$$

$$SD_F = \frac{SD_i - \overline{SD}}{\overline{SD}} \tag{5}$$

where *i* represents the individual measurements.

Snow density fraction and SD fraction data from snow pits and the AWS at this date were used to fit equation (6) by an ordinary least square algorithm:

$$\rho_i = \overline{\rho} \cdot \left(\frac{SD_i - \overline{SD}}{\overline{SD}} \right) \cdot k + \overline{\rho} \tag{6}$$

where *i* represents the individual measurements and *k* is the slope of the regression line.

The slope *k* of the linear function was found to be 0.23 (Figure 3) with in a high correlation represented by a r^2 value of 0.93. The local function could be verified with a r^2 value of 0.89 for the campaigns on 11 June 2015 and 24 November 2015, representing the melting season 2014/2015 and the beginning of the accumulation season 2015/2016, respectively. The within-site variation of snow density usually increases during snow melt with snow density becoming increasingly a function of liquid water content and refreezing of liquid water [*Jonas et al*., 2009; *López-Moreno et al*., 2013]. Thus, snow measurements made during the late melting season on 29 June 2015 and 29 June 2016 show an increased bias in the range of 5–12% when using equation (6) with a constant *k* value fitted with the data from 28 April 2016. This represents an increased uncertainty for the data of the late melt season but is still acceptable when compared to the literature [*Jonas et al*., 2009; *Schöber et al*., 2016].

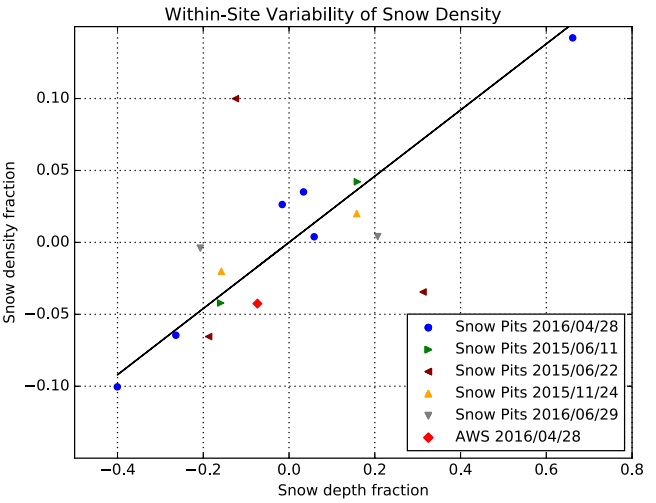

Figure 3. Measured within-site variations of snow density at snow pits (blue dots and colored triangles) and the automated weather station (red diamond) compared to within-site variations of snow depth.

Equation (6) was used to account for the effect of within-site variability of snow density for all TLS measurement campaigns. Therefore, the mean snow density $\overline{\rho}$ in kg m^{-3} is calculated from all available snow density measurements (AWS and snow pits) at the date of the campaign. Since automatic snow density measurements of the Snow-Pack-Analyzer are uncertain if SD is lower than 0.5 m only snow pit data were used for the campaigns on 24 November 2015 and 3 December 2015. Given a water density of 1000 kg m^{-3}, the distributed SWE in millimeter is calculated as a product of distributed SD in meter and snow density in kg m^{-3}. Therefore, the following equation is applied for each data point:

$$SWE_i = \rho_i \cdot SD_i \tag{7}$$

where i represents the elements of the SD grid.

3.3. Aboveground Neutron Sensing

The aboveground CRNS integrates information from an area of several hectares, referred to as intermediate scale. The CRNS is equipped with a ^{3}He proportional counter surrounded by a polyethylene moderator for the measurements of epithermal to fast natural neutrons created by a secondary cascade of cosmic rays. These neutrons interact with the land surface, and the signal is moderated by the hydrogen pools on the land surface. For this reason the monitoring of neutron counts well represents the temporal dynamics of water based on an inverse relation [*Zreda et al*., 2008; *Desilets et al*., 2010]. Due to the specific characteristic scattering length of neutrons in the atmosphere, the measurements integrate a signal over a large area in the order of hundreds of meters radius [*Desilets and Zreda*, 2013; *Köhli et al*., 2015]. For further information, readers may refer to *Zreda et al*. [2012].

In the present study, a CRNS (CRS-1000, Hydroinnova) [*Desilets et al*., 2010; *Zreda et al*., 2012] was installed in the period from March to June 2014 and was replaced by another sensor of the same model measuring from October 2014 to June 2016 (Figure 2). As the first sensor shows slightly higher count rates, a linear regression was applied for normalizing the data of both sensors. Differences between CRNS probes of the same model are common due to differences in the polyethylene shielding thickness or in the pressure of the Helium gas, which is usually solved by intercalibration [*Baatz et al*., 2015]. Both sensors were mounted at a height of 2.7 m above snow-free surface to prevent the CRNS to be buried by snow during peak accumulation conditions. The lowest distance between the senor's enclosure and snow surface was around 0.3 m in April 2015 (Figure 2b).

Raw neutron count rates were aggregated to hourly values and subsequently corrected for (i) incoming neutron intensity, (ii) air pressure, and (iii) absolute humidity according to the postprocessing for soil moisture applications [*Zreda et al*., 2012; *Rosolem et al*., 2013]. Data from the nearby neutron monitor Jungfraujoch in Switzerland (JUNG), which has the same geomagnetic cutoff rigidity, were used for correcting the variations in the neutron intensity. All additional data necessary for the corrections (i.e., air humidity, air temperature, and air pressure) were measured locally. For this reason they also well represent the specific environmental conditions. Neutron count rates generally follow a Poissonian distribution. With increasing neutron count rates, the uncertainty of the measurement relative to the total count rate decreases. Hence, hourly values would imply a high level of uncertainty during the period with large SWE values. For this reason, the corrected neutron count rates were averaged to 12 hourly values to increase the statistical accuracy of the measurements still partly capturing subdaily dynamics of snow properties.

3.4. Relating Neutron Counts to Snow Measurements

To investigate the characteristics of using CRNS for snow monitoring, both point-scale and distributed SD and SWE values are related to neutron counts. The coefficients a_0, a_1, a_2, and N_0 of a function originally developed for relating neutron counts to soil moisture [*Desilets et al*., 2010] are estimated by an ordinary least square algorithm using the respective subset of snow measurements:

$$f(N) = \frac{a_0}{\left(\frac{N}{N_0}\right) - a_1} - a_2 \tag{8}$$

SD and SWE predicted with the resulting function are compared to measured values. The Kling-Gupta-Efficiency (KGE) [*Kling et al*., 2012] was used as objective function as it includes r^2, a ratio of the coefficients of variation, and a bias ratio.

To test the temporal transferability of the resulting equations, a split sampling is applied. The data from the winter season 2014/2015 (11 samples) is used for calibrating the equations, while data for the winter seasons 2013/2014 and 2015/2016 is used for validation (7 samples). Therefore, point-scale SD and SWE values are reduced to dates with distributed snow measurements.

3.5. CRNS Footprint Over Snow

For characterizing the CRNS footprint, two different approaches were followed. In the first approach, the footprint was calculated using functions originally developed for soil moisture studies. Recently, the footprint characteristics were revised suggesting the use of a spatial weighting function to account for a time variant footprint and the spatial sensitivity of the signal [*Köhli et al*., 2015]. Every data point is weighted based on a spatial weighting function. In the present study, the reference pressure was set to 75 kPa, reference atmospheric moisture to zero. This weighting was originally developed only for soil moisture conditions. A soil moisture content of 99% was assumed to account for snow conditions as this reflects the near-saturation conditions of the snowpack. Snow-free data points are calculated assuming 20% of soil moisture. Due to the skeletal character of the soil, the latter value corresponds to rather wet conditions as assumed for the melting season. In theory, also other hydrogen pools reduce the footprint (and thus decrease the relative probability for neutrons in larger distance to the probe to be detected), while lower air pressure increases the footprint. However, only soil moisture and atmospheric moisture are implemented in the spatial weighting function. In a second step, the resulting radius of the theoretical footprint from where 86% of the neutrons originate is scaled by prefactors taking into account the effects of atmospheric pressure and a changing hydrogen pool stored in biomass. Due to the negligible seasonal effects of total hydrogen stored in biomass at the study site, the latter prefactor was held constant at a value of one. All distances were calculated in three dimensions to account for complex topography.

In the second approach, the footprint radius is estimated using a data-based optimization approach. The aim is to empirically verify the use of the theoretical approach for snow conditions. Another aspect is to test the temporal stability of the footprint at the study site. A simple, uniformly distributed average over all data points closer than the footprint radius f_{cal} to the CRNS is calculated. Neutron counts are compared to mean snow values within a specific randomly set radius. The parameters of equation (8) are estimated and a corresponding KGE value is calculated. To optimize f_{cal}, the radius is varied over a uniformly distributed space from 1 to 1000 m with 1999 samples. SD and SWE is processed separately using data from all campaigns. The respective calibrated uniform footprint f_{cal} for SD and SWE is defined as the distance with the highest KGE value. As data from all campaigns is included, high KGE values correspond to a temporally stable footprint. Due to the underlying uniform probability density function approach, slightly smaller values of the footprint radius are expected than for the theoretical approach.

4. Results and Discussion

4.1. Within-Site Variability of Snow Properties

The topography around the station consists of convex and concave features with differing surface roughness altering both the local wind field and the surface energy balance. Spatially heterogeneous snow accumulation and melt result in patchy snowpack depletion as shown in Figure 2. In sheltered areas snowpack typically persists a few weeks longer than at the AWS.

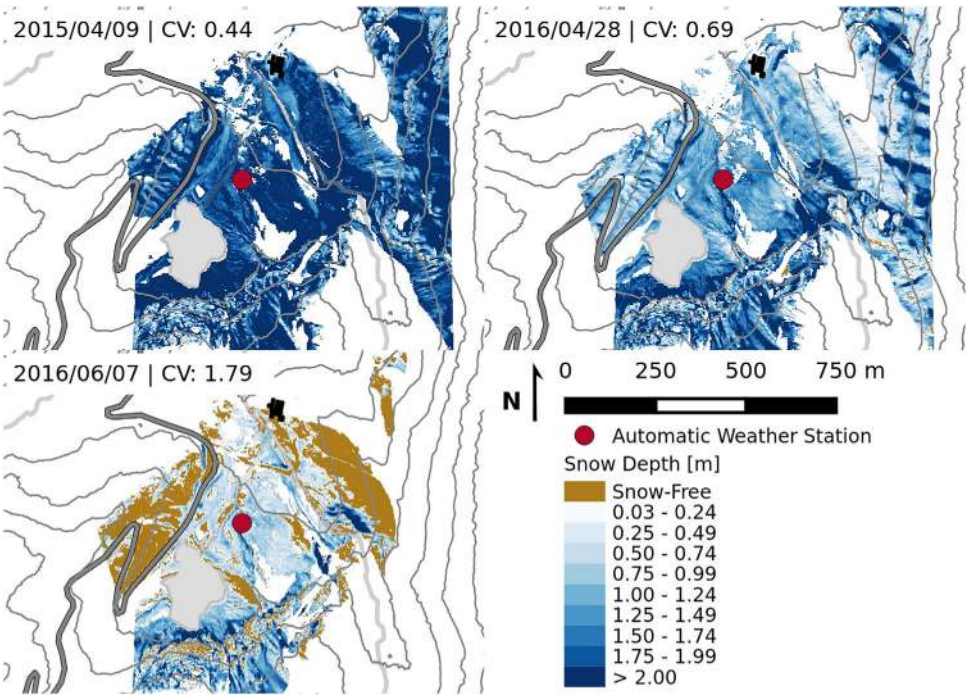

Figure 4. Temporal dynamics and within-site variations of SD. TLS maps for peak accumulation in 2015 and 2016 and the melting season 2016.

A known problem of point-scale SD measurements in alpine terrain is the representativeness as compared to mean values of larger areas [*Grünewald and Lehning*, 2015]. In the winter seasons 2013/2014 and 2014/2015, SD at the AWS was subject to strong wind-induced snow redistribution. TLS measurements in the 2014/2015 season indicate an overestimation of SD in the range of 23–129% at the AWS as compared to the mean values found in a 230 m radius. In contrast, in May 2014 AWS SD measurements were 42% below the mean SD value of the distributed campaign. In the winter season 2015/2016 measured SD values were closer to TLS derived means (deviations of -6 to $+15$%). This was very likely caused by a fence built around the station in summer 2015, and the geometrical reconfiguration of the Snow-Pack-Analyzer in August 2015 (see chapter 3.1), which had been orthogonal to the local wind field before.

The high within-site variability of the snowpack is visible in the TLS-derived distributed SD maps shown in Figure 4. To ensure a comparable spatial extent, only areas in the range of 230 m around the AWS are considered as the coverage of the outer areas differs for different TLS campaigns. As shown in Table 1, the percentage of snow-covered pixels during peak accumulation is very high. In 2015 a total of 98.5% of the data points within the 230 m radius were snow covered; in 2016 this was 96.5%. The corresponding CV values were higher in 2016. With the onset of spatially nonuniform snowpack depletion, snow coverage decreases to 63.5% in early June 2016, while the CV rises to 1.79.

4.2. Seasonal Evolution of the Snowpack

Snowpack evolution at the test site generally follows a typical alpine pattern with a long snow season from fall to midsummer (Figure 5). Whereas in October 2014 the accumulation period started quite early with a heavy storm, the 2015 accumulation period started rather late in December. After a step-wise snow accumulation period, peak accumulation in terms of SWE is typically reached in spring. Intermediate melt events occurred during fall and spring, e.g., in May 2015, in November 2015, in March 2016, and in April 2016. Yielding around 150 mm higher SWE values during peak accumulation, the winter 2014/2015 was considerably wetter than the winter 2015/2016. During the snow-free periods, three smaller snowfall events occurred during June 2014, July 2014, and September 2015.

While in general, the dynamics of SWE are related to variations in SD, seasonal differences arise from the evolution of bulk snow density. During accumulation snow densities ranged between 100 and 350 kg m^{-3}.

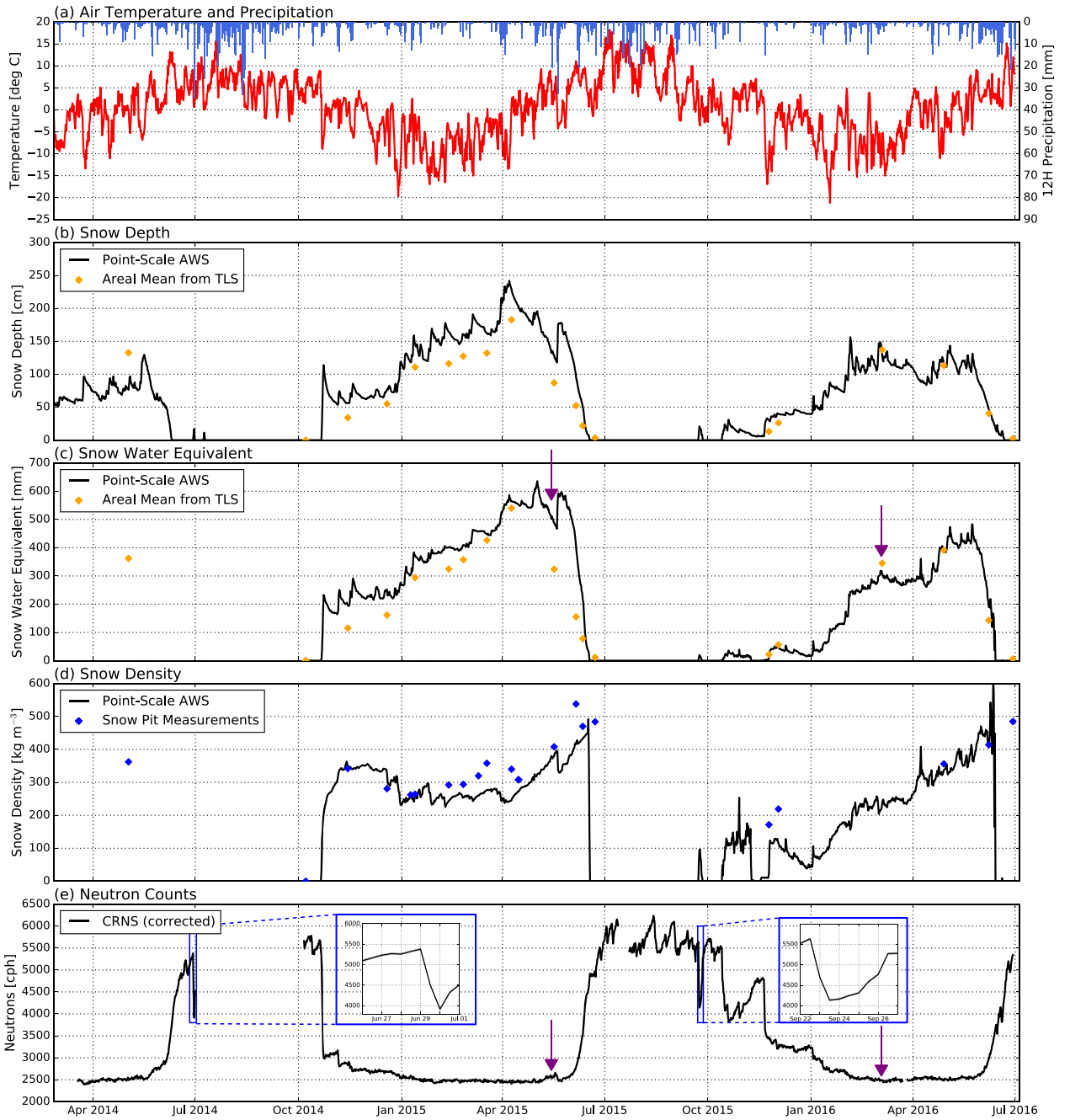

Figure 5. Seasonal snowpack evolution retrieved by a single point-scale measurement at the automated weather station (AWS) compared to the average value obtained from TLS (orange markers) and snow pit measurements (blue markers): (a) air temperature and precipitation (liquid and solid), (b) SD, (c) SWE where purple arrows mark two intermediate melt events, and (d) snow density. Measured 12 hourly corrected neutron count rates by CRNS are plotted in Figure 5e where purple arrows mark the same events as in Figure 5c. A subset of this plot shows neutron count rates after two snowfall events on snow-free ground with 22 cm (∼22 mm SWE) in June 2014 and 26 cm (∼26 mm SWE) in September 2015.

Melting snow was denser, with bulk densities of 400–550 kg m^{-3}, including a high content of liquid water in the pore space. Thus, due to the densification (compaction) of the snowpack with time and energy input, peak accumulation (in terms of SWE) does not usually correspond to the highest SD values. For a number of dates automatic snow density values are lower than the snow pit measurements. In June 2015 or November to December 2015, this was associated with SD values at the AWS below 0.5 m. Despite SD being above this level, similar differences between AWS snow density and manual measurements can be observed from January to May 2015 where automated measurements were hampered by air pockets around the sensor cable. After optimizing the location of the Snow-Pack-Analyzer with regard to the local wind field in August 2015,

both automatic and manual density measurements show better agreement, particularly during peak accumulation.

4.3. Seasonal Evolution of Neutron Counts

In Figure 5e the time series of 12 hourly neutron counts corrected for incoming neutron intensity, air pressure, and air humidity is shown for the whole study period. While in snow-free conditions measured neutron counts range between 5000 counts per hour (cph) during wet soil conditions, and 6240 during the peak of the August 2015 drought period, snow-covered conditions are characterized by considerably lower neutron count rates. Snowfall events cause a sharp decrease in neutron counts. Two snowfall events of around 20 cm of new snow (approximately 20 mm of SWE if assuming a new snow density of 100 kg m^{-3}) on 29 June 2014 and 29 September 2015 correspond both to a decrease in neutron counts of around 1500 cph each (subset of Figure 5e). The amplitude of the change between zero and 20 cm of snow cover is thus higher than the amplitude between wet and dry soil conditions. For both snowfall events, neutron counts fell below the level of wet soil conditions, an effect that could be useful for phase detection of precipitation by applying a threshold. The pronounced decrease of count rates reported also by other studies is due to the presence of relatively large amounts of hydrogen in snow compared to soil, in which the amount of water is limited by the porosity of the soil matrix. Furthermore, in soil the grain material can contribute significantly to the neutron attenuation. This creates a background that is weakening the dynamics of the neutron response to water content changes. In snow, however, the neutrons do not interact with the air inside the snow, and only water—frozen, liquid, or as vapor—is contributing to the signal. An experimental study in the French Alps showed however that in the presence of snow neutron fluxes can be reduced even more than can be explained by hydrogen mass alone which was attributed to possible boundary effects [*Delunel et al*., 2014]. Still, absolute levels of neutron counts after snowfall depend on preevent count rates. This confirms findings from other studies reporting a mixed signal of soil moisture and snow for shallow snowpacks below approximately 30 mm of SWE [*Franz et al*., 2012b; *Zweck et al*., 2013; *Delunel et al*., 2014; *Sigouin and Si*, 2016]. For deeper snowpacks, this effect is expected to be negligible.

The winter seasons correspond to periods with generally lower count rates. As for soil moisture, the slope of neutron count decrease in fall is steeper than for count rate recovery in summer. Decreases are triggered by short-lived precipitation events, whereas increases are due to drying of soil or melting of snow which are longer-lived events. Even for high values of SD, the neutron signal is not completely saturated. The accumulation and melt-out phases in fall and summer have their correspondence in neutron count rates. The neutron signal also allows for tracing intermediate snowfall and melt events like on May 2015 or March 2016. Even with high SD values during peak accumulation, neutron count rates never drop below 2000 cph. An amount corresponding to around one third of the neutron count rate for dry conditions is produced in the top snow layer during snow-covered conditions.

4.4. Estimating the Footprint Characteristics Over Snow

The footprint radius is relatively stable over time for the atmospheric and meteorological conditions at the study site. The theoretical equation [*Köhli et al*., 2015] for homogeneous conditions over snow is dominated by the absolute humidity being generally rather low. In summer, the theoretical footprint over snow defined as the distance from where 86% of neutrons originate is 247 m. The 63% of neutrons originate within a distance of 85 m. The inner footprint from where 50% of the neutrons originate is 41 m. Due to lower humidity at low temperatures, the corresponding values are slightly higher during the winter period (273, 102, and 49 m).

Optimizing the uniform footprint f_{cal} for SD and SWE revealed higher overall KGE values for SD but very similar distance-dependent patterns of KGE values (Figure 6). The generally lower KGE values for SWE data result from a different shape of the function describing the relation between neutron counts and SWE during the melting period (see chapter 4.5). Very small averaging distances exhibit the lowest KGE values. A first local maximum can be found for a radius of 15 m, followed by a local minimum at 32 m. The best fit, indicated by the highest KGE, was found at around 230 m for both SD and SWE. The data sets from all measurement campaigns were used in the optimization. The good fit therefore indicates a stable footprint over time.

Both the theoretical and the empirically optimized approaches hence show comparable results, as due to the differences in the underlying probability density functions, the averaging radius of the uniform averaging is likely to be smaller than the radius of the theoretical footprint. This indicates that footprint functions

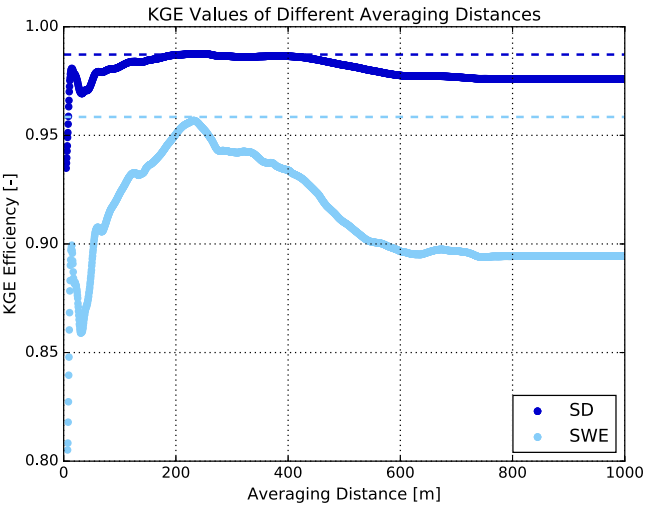

Figure 6. Optimization of the calibrated uniform footprint f_{cal} for SD and SWE based on all campaigns. The corresponding KGE value if using the spatial weighting function is indicated by dotted horizontal line, respectively.

developed for soil moisture also give realistic results for snow-covered conditions. Another interesting aspect is that the high altitude of the site results in low atmospheric pressure and small atmospheric hydrogen pools, which enlarges the footprint and partly compensates for the effect of the large hydrogen pool in snow that shrinks the footprint.

4.5. Correlating Neutron Counts to Snow Properties

Corrected neutrons counts are compared to the snow measurements conducted at different spatial scales, i.e., point-scale data and distributed campaigns based on TLS (Figure 7). To account for the different number of available data sets, only the point-scale data obtained at the time of distributed campaigns are considered. In general, agreements between neutron counts and snow measurements are high over the complete range of SD and SWE values following highly nonlinear functions. This type of function was also found for soil moisture. A plausible explanation for the different function type found by *Sigouin and Si* [2016] could be the limited amount of snow in their study. If considering only a subset of the data in the range that was observed in that study, a linear function could be fitted. The good fit of SD is surprising as neutron fluxes should be affected by hydrogen mass only.

The penetration depth in snow appears to be deeper than in pure water or soil. The role of spatial structure of hydrogen distribution on neutron counts could be a possible explanation that is supported by a recent modeling study [*Andreasen et al*., 2017]. In that study the impact of different structures on neutron counts has been investigated quantitatively, however, only with respect to forest biomass. In heterogeneous alpine terrain, the distribution of high SWE values is highly variable in space, where large changes of SWE can occur even within few decimeters of distance. For this reason, further studies should be conducted focusing on the role of the strong spatial variability of SWE in alpine terrain on neutron fluxes.

The advantages of CRNS to measure snowpack properties with a high spatial variability can be illustrated comparing SD and SWE on different spatial scales, respectively. Considering SD, the point-scale measurements show the same nonlinear relation and good fit as compared to the TLS measurements (Table 2). The main difference is observable as an offset from the curve for the melting season 2014/2015. This is consistent with the constant overestimation detected between the point measurements and the TLS campaigns (see Figure 5b). Considering SWE, the correlation between point-scale measurements and neutron counts are less pronounced. The interannual differences are larger than for SD. With distributed data, this effect disappears, confirming that the CRNS measurements are not affected by small-scale heterogeneities.

Considering distributed SD and SWE, the differences between the two different approaches for averaging the distributed measurements are smaller than in soil moisture studies [*Köhli et al*., 2015; *Heidbüchel et al*., 2016]. This is probably caused by the high number of data points, the relative stability of the footprint radius in time and the fact that the support distance was explicitly calibrated for the test site. Another possible factor could be the near saturation of the signal in the presence of snow in contrast to a high variability of the signal with changing soil moisture dynamics. Still, it is noteworthy that the spatial weighting slightly improves the results. For operational snow monitoring, averaging over a fixed distance could however be easier to implement.

With distributed SWE data, different curves for the accumulation and for the melting period become evident. The offset is larger than the uncertainty introduced by neutron counts or snow measurements. The uncertainty of the SWE data increases during the melting period due to the constant k factor in equations (6) and (7). However, resulting potential errors are in the range of few mm of SWE for the area estimate. A

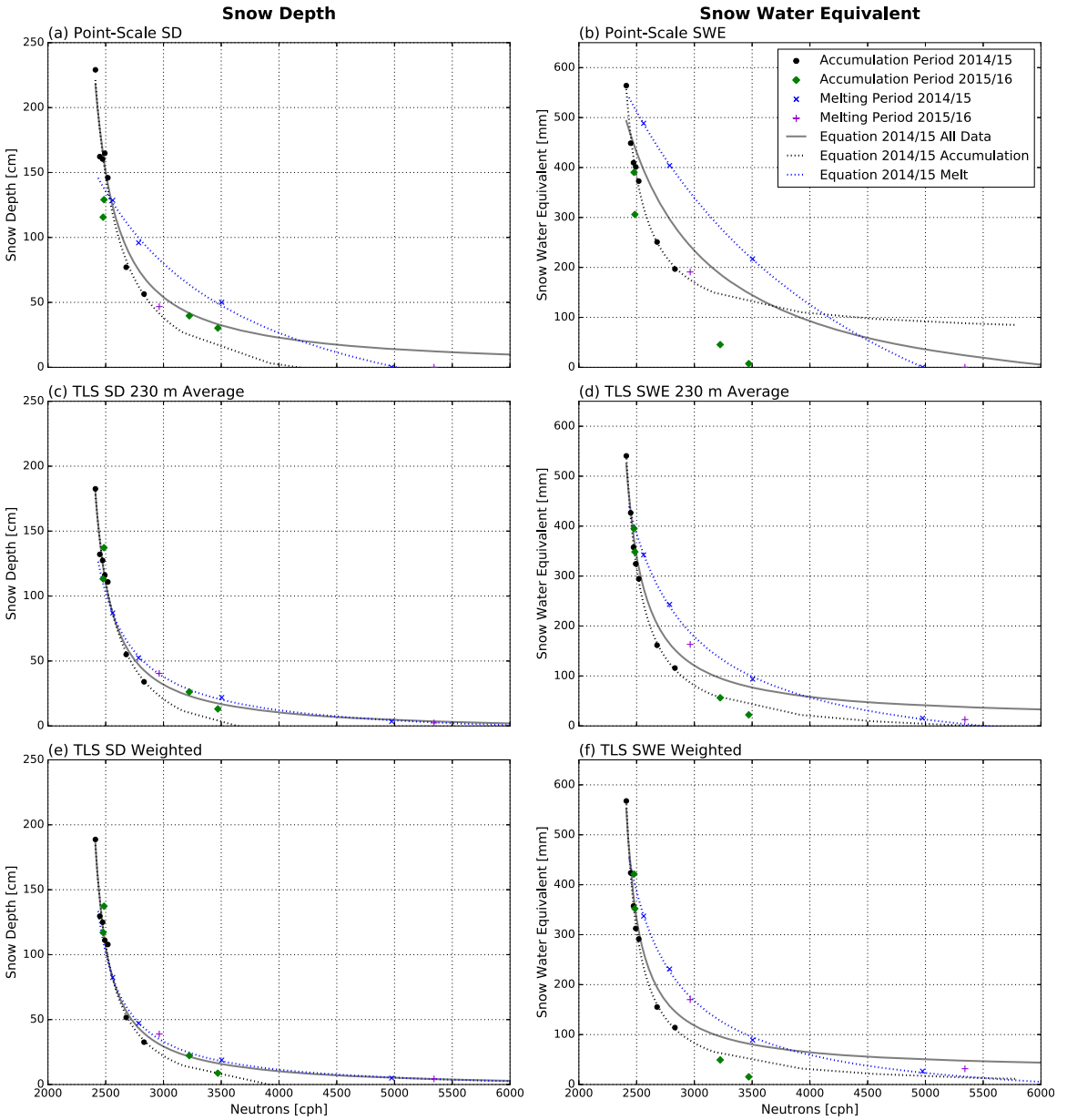

Figure 7. Different calibration curves of neutron counts (cph) versus the two snow properties observed during snow measuring campaigns: derived from (a) point-scale SD, (b) point-scale SWE, (c) distributed TLS SD averaged over a 230 m radius around the AWS, (d) distributed TLS SWE averaged over a 230 m radius around the AWS, (e) spatially weighted distributed SD, and (f) spatially weighted distributed TLS SWE.

possible explanation could be that count rates are shifted toward (higher) snow-free levels due to the presence of snow-free patches. The result is a mixed signal of low snow-affected count rates and high snow-free count rates. This effect is however minimized by using distributed SD and SWE data and spatially weighting the data. The spatial weighting function [*Köhli et al.*, 2015] accounts for the effect of averaging nonlinear data by including a higher contribution from the snow-free patches. Still, different curves were found for the accumulation and the melting season, suggesting that some aspects of neutron interactions with different layers of snow and soil, like edge effects or the spatial heterogeneity of the snowpack, are not accounted for.

Another aspect points to varying snow density leading to altered interactions with neutrons. Snow structure and density could decrease the effective measurement depth as was shown for soil moisture [*Franz et al.*, 2012a; *Köhli et al.*, 2015]. Snow density is generally lower during the accumulation period. During the

Table 2. KGE Values of Fitting Measured Snow Data to Neutron Counts in the Calibration Period

	All Data	Accumulation Period	Melting Period
Snow depth point-scale	0.972	0.985	0.998
Snow depth TLS 230 m	0.993	0.992	0.999
Snow depth TLS weighted	0.993	0.992	0.999
SWE point-scale	0.895	0.995	0.999
SWE TLS 230 m	0.960	0.999	0.999
SWE TLS 230 m corrected	0.986	0.999	0.990
SWE TLS weighted	0.962	0.962	0.999
SWE TLS weighted corrected	0.996	0.999	0.998

melting season bulk density values above 450 kg m^{-3} were associated with high liquid water contents. To empirically test this hypothesis, a limitation of effective measurement depth was introduced:

$$SWE_i = \begin{cases} \min\ (SWE_i, d), & \rho_i > p \\ SWE_i, & \rho_i \leq p \end{cases} \quad (9)$$

The correction was developed with data from the 2014/2015 season by manually calibrating thresholds for effective measurement depth d and critical snow density p. Best results were obtained with a measurement depth limit at 200 mm for all data points where snow density exceeds 450 kg m^{-3}. Applying the measurement depth limit for all data sets resulted in worse agreements, as did higher or lower thresholds for both parameters. The measurement depth-corrected SWE values show a unique function for all data points including the melting season as shown in Figure 8. The measurement depth-corrected SWE values also show reasonable results for the validation period 2015/2016.

Most likely the effective measurement depth decreases nonlinearly as more pore spaces become filled with liquid water, which has the largest effects for very dense snow where most pore spaces are occupied. This is mimicked by the threshold function. As the function was derived empirically, no information could be obtained however about the actual physical processes in terms of neutron interactions or the form of the associated mathematical function. A universal function should be derived from neutron modeling. To enhance the empirical data base with data from different sites, it is therefore recommended to include field samples of SD, snow density, and liquid water content from both the accumulation and the melting period into the study design.

The data presented in this study give empirical evidence that neutron fluxes measured by the aboveground probe show snow-related signals even for a comparably deep snowpack of up to 600 mm of SWE. A buried probe, better suited for deeper snowpacks, was reported to be capable of measuring SWE values up to 1–12 m when measuring in the range of 1 eV–1 MeV [*Kodama*, 1984]. But a buried probe is only a very local measurement, and therefore CRNS measurements appear to be more robust for applications in heterogeneous alpine terrain. In addition, measuring 12 m of SWE by a buried probe seems to be highly unlikely given the attenuation length of neutrons in snow for the neutron energies targeted by the sensor. For this reason, the limits of saturation of the CRNS and a buried probe could be much more comparable.

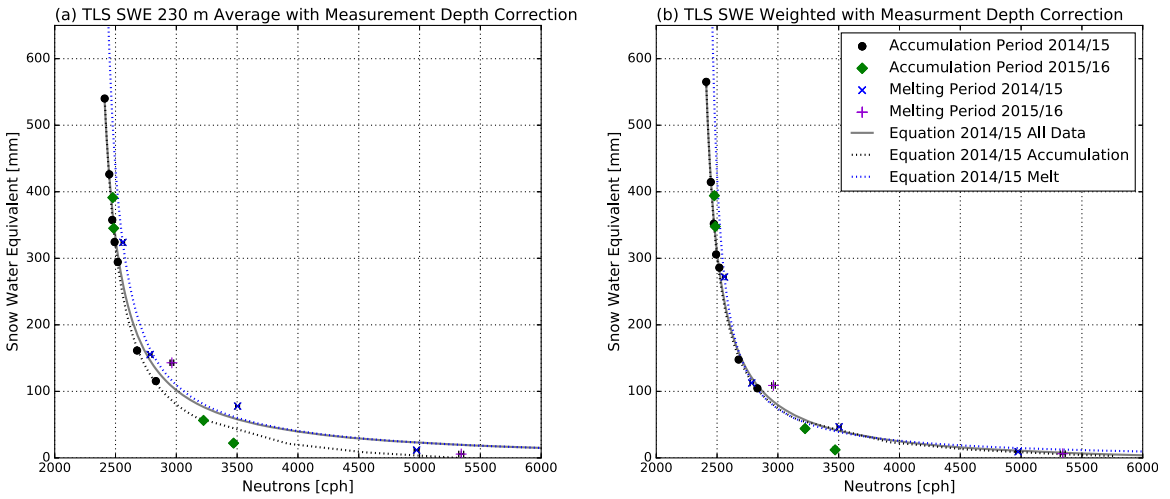

Figure 8. Calibration curves of neutron counts (cph) and measurement depth-corrected SWE values from (a) a 230 m average and (b) spatially weighted data.

Table 3. KGE Values of Predicting Snow Values in the Validation Period

	All Data	Accumulation Period	Melting Period
Snow depth point-scale	0.593	0.666	0.258
Snow depth TLS 230 m	0.924	0.922	0.823
Snow depth TLS weighted	0.897	0.919	0.811
SWE point-scale	0.362	0.565	0.264
SWE TLS 230 m	0.894	0.918	0.915
SWE TLS 230 m corrected	0.939	0.924	0.808
SWE TLS weighted	0.890	0.868	0.891
SWE TLS weighted corrected	0.914	0.881	0.789

The fitted functions generally have a very high agreement in terms of KGE with observed data (Table 2). The spatial weighting function slightly increases the fit. Uniformly averaged point-scale and TLS data show slightly lower efficiency values than spatially weighted data, but regardless of the weighting, TLS data fit considerably better than point-scale data.

To test interannual transferability, the resulting functions were used to predict the observed data in the validation period that is the winter seasons 2013/2014 and 2015/2016. While the functions for point-scale measurements are not well suited to predict SD and SWE in the validation period, the functions for spatially distributed values are transferable (Table 3). Distributed data corrected for measurement depth show the best interannual transferability. Considering both the accumulation and melting seasons, the functions based on spatially weighted data with measurement correction are most robust as indicated by very high KGE values.

4.6. Performance of Snowpack Monitoring via CRNS

The reconstruction of SD and SWE values for the entire time series using corrected neutron counts is illustrated in Figure 9. The functions were developed including only the data from the 2014/2015 snow season using spatially weighted, measurement depth-corrected snow measurements. For all dates of snow measurement campaigns (Table 1), SD derived via CRNS matches the mean value in the study area better than the point-scale measurements at the AWS. Furthermore, the CRNS-derived values are almost always in excellent agreement with the values from the campaign, with only the March 2014 campaign slightly differing to the value from the campaign. However, this was the only campaign not using the TLS but snow sticks at 30 points, and the conclusion could also be that this is not as representative as the TLS-measured values, and the CRNS-derived value may well be correct. The CRNS-derived values perform equally well for snow water equivalent. In two cases, the point-measurement matches exactly the TLS-derived average. Since it is off otherwise, this may rather be a coincidence. But even during peak accumulation, the CRNS-derived value

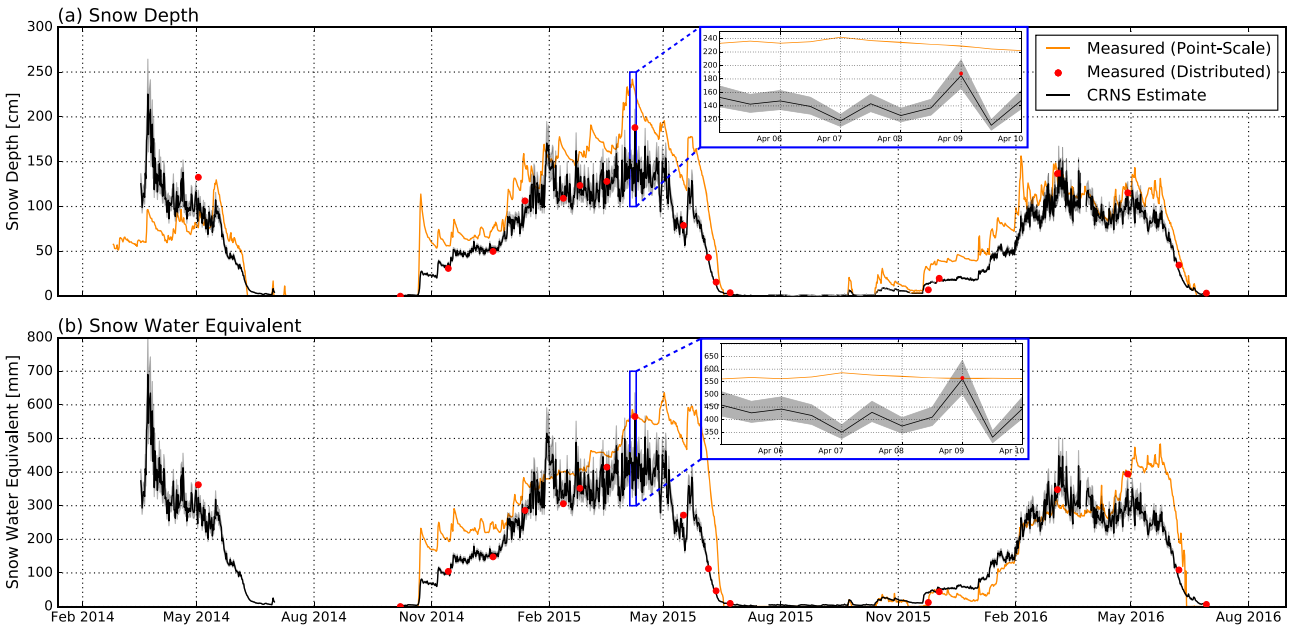

Figure 9. (a) SD and (b) SWE data reconstructed from neutron counts using the equations developed for the season 2014/2015 compared to measured snow data. The range of uncertainty induced by neutron counting statistics is shown as shaded area.

always matches well or at least is acceptable within the neutron count-induced statistical uncertainty, plotted as shaded area. However, during periods with high accumulation with SWE values above around 400 mm, the signal appears to be close to saturation, particularly during the winter season 2014/2015 (subset of Figure 9). It seems clear that CRNS, once calibrated, can reproduce well the dynamic snowpack evolution during the whole snow season. In snow-free conditions during summer, a small background remains that is very likely caused by soil moisture as to be expected. Nevertheless, even comparably small intermittent snow-fall events during that period create a signal exceeding the background and therefore could correctly be distinguished and identified.

Overall, CRNS proves therefore to be remarkably well suited for monitoring mountain snowpacks. Still, some additional discussion is necessary to better understand the reliability of the measurements. The uncertainty of estimating SWE or SD generally increases with increasing snowpack. This is due to the combined effects of a higher statistical uncertainty at lower count rates and the steep slope of the function relating neutron counts to SD and SWE. The uncertainty can be reduced by increasing the time step of neutron counts measurements. For hourly values and snowpacks above 300 mm of SWE or 1 m of SD, the combined effects of high statistical uncertainty at low count rates and the steepness of the function would translate into high errors in the range of up to 30–40%. Using 12 hourly data reduces the uncertainty of estimating SWE and SD induced by statistical neutron count errors to a level 1–12%, with an average of 4%. The corrections applied to the raw neutron count rates could provide additional sources of uncertainty. However, the corrections in this study are based on the incoming neutron data provided by a monitoring station relatively close to the experimental site, and on meteorological data collected directly at the experimental site. For these reasons, the uncertainty introduced by these corrections is expected to be lower than the other sources of uncertainty.

Another important limitation is the near saturation of the signal for high values of SWE and SD. Given the form of the functions relating neutron counts to SD and SWE, the signal seems to be saturated at around 600 mm of SWE and 2 m of SD, respectively. Already at around 400 mm of SWE and 120 cm of SD, high noise is present in the reconstructed SWE and SD values, which cannot be explained by the uncertainty of neutron counts and its corrections alone (see Figure 9). A larger time step, as was used in this study, is therefore recommended when the snowpack is deeper than 200 mm. This is particularly important in environments with low overall count rates like low altitude locations.

5. Conclusions

The presented experiment at an alpine site with a snowpack of up to 600 mm of SWE proves that CRNS is suitable for monitoring snow in complex mountainous terrain. Even for SWE values considerably higher than the 100 mm presumed so far in literature, no complete saturation of the neutron signal is found. A mixed signal of snow and soil moisture was observed for shallow snowpack in agreement with other studies [*Zweck et al*., 2013; *Sigouin and Si*, 2016]. Moreover, snowfall events can be distinguished from rainfall events in the summer period since the decrease of neutron fluxes by snow is more pronounced than by wet soil. This opens an interesting application to detect the elevation of the snowline which has a large impact on flood generation.

Both SD and SWE show a strong correlation with neutron count rates following a highly nonlinear function. This relationship between neutron counts and snow properties can be represented by the function usually used for the soil water content measurement by CRNS, though with different parameter values. Separate functional parameterizations were found to describe the relation between neutron fluxes and SWE during the accumulation and melting periods. To resolve the issue of having two different functional parameterizations, a detection limit at 200 mm of SWE for very high snow densities above 450 kg m^{-3} was introduced. The empirically based measurement depth limitation resulted in a unique function with a far better overall fit. Still, the underlying mechanism itself was not yet analyzed or described by means of a physical neutron scattering model. For comparing SWE or SD derived via CRNS with other snow data, it is important to identify the areas where to apply the measurement depth limitation. As proxies for these areas, potentially both in situ measurements of snow density or liquid water content and remote sensing-based snow wetness maps could be useful. As both functions converge at peak SWE conditions, an alternative option is using seasonally different functions for converting neutron counts in SWE.

As both SD and SWE are highly variable in space, and the probability of a neutron to be detected is a function of distance, best correlation results have been achieved for spatially weighted LiDAR-derived snow data (KGE $>$ 0.99). A good interannual transferability of the relationship between neutron counts and distributed snow data was found. This corresponds to KGE values in the validation period of 0.897 for SD and 0.914 for SWE. In contrast, point-scale SD and SWE values show lower correlations with neutron counts, and the derived equations perform considerably worse in the validation period. This corresponds to CRNS representing indeed a SD and SWE averaged over an extended support area. This footprint depends in general on air humidity, soil moisture, and snow cover itself. Values in larger distance contribute somewhat less to the signal, which was accounted for by spatial weighting. As long as the CRNS probe is above the snow cover, the shielding of neutrons by the snow cover is only indirect and results in a moderate influence on the footprint size. Otherwise snow directly around the CRNS probe will eliminate some of the neutrons to be counted, which should be avoided by installation of the CRNS probe above the local maximum snow cover. The average footprint during the season, based on measurements over almost three snow seasons, was estimated to be around 230 m.

The large support of the CRNS underlines its advantages over conventional point-scale snow measurements, as point-scale data may not be representative for its surrounding area (Figure 7). Thus, CRNS seems to have clearly the potential to become an excellent method for representative continuous measurement of average SD and SWE. Possible applications include intermediate-scale snow monitoring for water resource management, runoff forecasting, or multiobjective calibration of hydrological models. Another potential application is using CRNS measurements as automated "ground truth" for satellite data [*Lundberg et al*., 2010].

Assuming that the background conditions are less relevant in snow-covered conditions than in snow-free conditions, the transferability of the relation for snow measurements might be better than for soil moisture applications. However, as this study was carried out at a single location, this needs to be investigated. Further research is also needed for understanding possible differences in neutron intensities between accumulation and melting periods. Dedicated neutron modeling with spatially heterogeneous SD and SWE scenarios could help to understand the interactions of neutrons at the interface of atmosphere, snowpack, and soil. This would also give more insight into the characteristics of the CRNS footprint under snow conditions. Another aspect that could be addressed by both modeling and experimental studies is including the information of thermal neutron counts as was suggested by preliminary experimental studies [*Rivera Villarreyes et al*., 2011; *Tian et al*., 2016] and a neutron modeling study [*Andreasen et al*., 2017]. This would include the use of an additional bare neutron counter which can be optionally installed in the same enclosure. Thermal neutrons are expected to contribute additional information on snow, at least as indicator for the presence of snow but their behavior with increasing snowpack still needs to be explored. Finally, data from field experiments and neutron modeling could be used to extend the COSMIC operator [*Shuttleworth et al*., 2013] for snow conditions, enabling the assimilation of snow states and the partitioning of the hydrogen pools in soil and snow. Further research should also address the added value of CRNS-derived SWE for snow-hydrological applications as compared to other snow data. A multiobjective hydrological model calibration could e.g., show the impact on reducing parameter uncertainty or the reconstruction of basin-wide SWE.

Acknowledgments

This work was carried out as part of the project "W02 HoPI III-Runoff Forecasting System for the Inn River" at alpS – Centre for Climate Change Adaptation in Innsbruck, Austria. The K1-Centre alpS is funded through the Federal Ministry of Transport, Innovation and Technology (BMVIT), the Federal Ministry of Science, Research and Economy (BMWFW), as well as the Austrian Provinces of the Tyrol and Vorarlberg within the scope of COMET – Competence Centers for Excellent Technologies. The Programme COMET is managed by the Austrian Research Promotion Agency (FFG). The project is cofunded by TIWAG-Tiroler Wasserkraft AG. The contribution of P. Schattan and M. Huttenlau were funded within the scope of the project "W02 HoPI III," J. Schöber is company researcher in this project. The contribution of J. Schöber and C. Fey was funded by TIWAG Tiroler Wasserkraft AG. S. Achleitner is responsible Key Research in the project "W02 HoPI III," his contribution was part of his employment at the University of Innsbruck as permanent staff. G. Baroni had financial support from the Deutsche Forschungsgemeinschaft (DFG) under CI 26/13-1 in the framework of the research unit FOR 2131 "Data Assimilation for Improved Characterization of Fluxes across Compartmental Interfaces." The contribution of C. Kormann was funded through the Postgraduate Scholarship of the University of Potsdam. The contribution of S. Oswald was part of his employment as full Professor for Water and Matter Transport in Landscape at the University of Potsdam. We thankfully acknowledge the University of Potsdam for providing the CRNS for this study which was funded via EFRE-HIP-Brandenburg 80158356. The NMDB database (www.nmdb.eu), founded under the European Union's FP7 7th Framework Programme (contract 213007) and the University of Bern are acknowledged for providing neutron monitor data. Furthermore, we acknowledge TIWAG-Tiroler Wasserkraft AG for providing environmental data for the study site. We specially thank Sebastian Sprenger (master thesis, University of Innsbruck) for his support during the TLS campaigns in the season 2014/15. We would like to thank Till Francke and Robert Kirnbauer for helpful discussions. The authors declare not having any conflicts of interest. The data discussed in this paper are available in the figures, tables, references, and the supporting information of this work. Raw data of neutron counts and snow measurements are available upon request.

References

Andreasen, M., K. H. Jensen, D. Desilets, M. Zreda, H. R. Bogena, and M. C. Looms (2017), Cosmic-ray neutron transport at a forest field site: The sensitivity to various environmental conditions with focus on biomass and canopy interception, *Hydrol. Earth Syst. Sci.*, *21*(4), 1875–1894, doi:10.5194/hess-21-1875-2017.

Avdyushin, S. I., E. V Kolomeyets, I. M. Nazarov, A. N. Pegoyev, and S. D. Fridman (1982), Application of cosmic rays to the solution of some hydrological problems, Proceedings of the Exeter Symposium, *IAHS Publ.*, *138*, 155–160.

Baatz, R., H. R. Bogena, H.-J. Hendricks Franssen, J. A. Huisman, C. Montzka, and H. Vereecken (2015), An empirical vegetation correction for soil water content quantification using cosmic ray probes, *Water Resour. Res.*, *51*, 2030–2046, doi:10.1002/2014WR016443.

Baatz, R., H.-J. Hendricks Franssen, X. Han, T. Hoar, H. R. Bogena, and H. Vereecken (2016), Evaluating the value of a network of cosmic-ray probes for improving land surface modelling, *Hydrol. Earth Syst. Sci., Discuss.*, 1–36, doi:10.5194/hess-2016-432.

Baroni, G., and S. E. Oswald (2015), A scaling approach for the assessment of biomass changes and rainfall interception using cosmic-ray neutron sensing, *J. Hydrol.*, *525*, 264–276, doi:10.1016/j.jhydrol.2015.03.053.

Berezowski, T., J. Chormański, and O. Batelaan (2015), Skill of remote sensing snow products for distributed runoff prediction, *J. Hydrol.*, *524*, 718–732, doi:10.1016/j.jhydrol.2015.03.025.

Bhardwaj, A., L. Sam, A. Bhardwaj, and F. J. Martín-Torres (2016), LiDAR remote sensing of the cryosphere: Present applications and future prospects, *Remote Sens. Environ.*, *177*, 125–143, doi:10.1016/j.rse.2016.02.031.

Blöschl, G. and M. Sivapalan (1995), Scale issues in hydrological modelling: A review, *Hydrol. Processes*, *9*, 251–290, doi:10.1002/hyp.3360090305.

Bogena, H. R., J. A. Huisman, R. Baatz, H.-J. Hendricks Franssen, and H. Vereecken (2013), Accuracy of the cosmic-ray soil water content probe in humid forest ecosystems: The worst case scenario, *Water Resour. Res.*, *49*, 5778–5791, doi:10.1002/wrcr.20463.

Bühler, Y., M. Marty, L. Egli, J. Veitinger, T. Jonas, P. Thee, and C. Ginzler (2015), Snow depth mapping in high-alpine catchments using digital photogrammetry, *Cryosphere*, *9*(1), 229–243, doi:10.5194/tc-9-229-2015.

Choquette, Y., P. Ducharme, and J. Rogoza (2013), CS725, an accurate sensor for the snow water equivalent and soil moisture measurements, in *International Snow Science Workshop Grenoble—Chamonix Mont-Blanc—7–11 October*, pp. 931–936, Montana State Univ., Bozeman, Mont.

Clifford, D. (2010), Global estimates of snow water equivalent from passive microwave instruments: History, challenges and future developments, *Int. J. Remote Sens.*, *31*(14), 3707–3726, doi:10.1080/01431161.2010.483482.

Deems, J. S., T. H. Painter, and D. C. Finnegan (2013), Lidar measurement of snow depth: A review, *J. Glaciol.*, *59*(215), 467–479, doi:10.3189/2013JoG12J154.

Deems, J. S., P. J. Gadomski, D. Vellone, R. Evanczyk, A. L. LeWinter, K. W. Birkeland, and D. C. Finnegan (2015), Mapping starting zone snow depth with a ground-based lidar to assist avalanche control and forecasting, *Cold Reg. Sci. Technol.*, *120*, 197–204, doi:10.1016/j.coldregions.2015.09.002.

Delunel, R., D. L. Bourles, P. A. van der Beek, F. Schlunegger, I. Leya, J. Masarik, and E. Paquet (2014), Snow shielding factors for cosmogenic nuclide dating inferred from long-term neutron detector monitoring, *Quat. Geochronol.*, *24*, 16–26, doi:10.1016/j.quageo.2014.07.003.

Desilets, D. (2014), Using COSMOS sensors to measure snow water equivalent on the ground and in the forest canopy, Abstract 14424 presented at 2014 General Assembly 2014, EGU, Vienna, Austria, 27 Apr.—2 May.

Desilets, D., and M. Zreda (2013), Footprint diameter for a cosmic-ray soil moisture probe: Theory and Monte Carlo simulations, *Water Resour. Res.*, *49*, 3566–3575, doi:10.1002/wrcr.20187.

Desilets, D., M. Zreda, and T. P. A. Ferré (2010), Nature's neutron probe: Land surface hydrology at an elusive scale with cosmic rays, *Water Resour. Res.*, *46*, W11505, doi:10.1029/2009WR008726.

Dietz, A. J., C. Kuenzer, U. Gessner, and S. Dech (2012), Remote sensing of snow: A review of available methods, *Int. J. Remote Sens.*, *33*(923037131), 4094–4134, doi:10.1080/01431160500219018.

Dozier, J. (1989), Estimation of properties of alpine snow from landsat thematic mapper, *Adv. Space Res.*, *9*(1), 207–215, doi:10.1016/0273-1177(89)90487-0.

Egli, L., T. Jonas, and R. Meister (2009), Comparison of different automatic methods for estimating snow water equivalent, *Cold Reg. Sci. Technol.*, *57*(2–3), 107–115, doi:10.1016/j.coldregions.2009.02.008.

Finger, D., F. Pellicciotti, M. Konz, S. Rimkus, and P. Burlando (2011), The value of glacier mass balance, satellite snow cover images, and hourly discharge for improving the performance of a physically based distributed hydrological model, *Water Resour. Res.*, *47*, W07519, doi:10.1029/2010WR009824.

Finger, D., M. Vis, M. Huss, and J. Seibert (2015), The value of multiple data set calibration versus model complexity for improving the performance of hydrological models in mountain catchments, *Water Resour. Res.*, *51*, 1939–1958, doi:10.1002/2014WR015712.

Franz, T. E., M. Zreda, T. P. A. Ferre, R. Rosolem, C. Zweck, S. Stillman, X. Zeng, and W. J. Shuttleworth (2012a), Measurement depth of the cosmic ray soil moisture probe affected by hydrogen from various sources, *Water Resour. Res.*, *48*, W08515, doi:10.1029/2012WR011871.

Franz, T. E., M. Zreda, S. Jones, and J. Carlisle (2012b), Measurement of hydrogen pools at intermediate spatial scales using cosmic-ray neutron probes at the T. W. Daniel experimental forest instrumented research site, in *Spring Runoff Conference*, pp. 838–491.

Franz, T. E., A. Wahbi, M. Vreugdenhil, G. Weltin, L. Heng, M. Oismueller, P. Strauss, G. Dercon, and D. Desilets (2016), Using cosmic-ray neutron probes to monitor landscape scale soil water content in mixed land use agricultural systems, *Appl. Environ. Soil Sci.*, *2016*, 1–11, doi:10.1155/2016/4323742.

Frei, A., M. Tedesco, S. Lee, J. Foster, D. K. Hall, R. Kelly, and D. A. Robinson (2012), A review of global satellite-derived snow products, *Adv. Space Res.*, *50*(8), 1007–1029, doi:10.1016/j.asr.2011.12.021.

Goodison, B. E., J. E. Glynn, K. D. Harvey, and J. E. Slater (1987), Snow surveying in Canada: A perspective, *Can. Water Resour. J.*, *12*(2), 27–42, doi:10.4296/cwrj1202027.

Grünewald, T., and M. Lehning (2015), Are flat-field snow depth measurements representative? A comparison of selected index sites with areal snow depth measurements at the small catchment scale, *Hydrol. Processes*, *29*(7), 1717–1728, doi:10.1002/hyp.10295.

Gutmann, E. D., K. M. Larson, M. W. Williams, F. G. Nievinski, and V. Zavorotny (2012), Snow measurement by GPS interferometric reflectometry: An evaluation at Niwot Ridge, Colorado, *Hydrol. Processes*, *26*(19), 2951–2961, doi:10.1002/hyp.8329.

Hall, D. K., G. A. Riggs, and V. V. Salomonson (1995), Development of methods for mapping global snow cover using moderate resolution imaging spectroradiometer data, *Remote Sens. Environ.*, *54*(2), 127–140, doi:10.1016/0034-4257(95)00137-P.

Hall, D. K., G. A. Riggs, V. V. Salomonson, N. E. DiGirolamo, and K. J. Bayr (2002), MODIS snow-cover products, *Remote Sens. Environ.*, *83*(1), 181–194.

Hartzell, P. J., P. J. Gadomski, C. L. Glennie, D. C. Finnegan, and J. S. Deems (2015), Rigorous error propagation for terrestrial laser scanning with application to snow volume uncertainty, *J. Glaciol.*, *61*(230), 1147–1158, doi:10.3189/2015JoG15J031.

Heidbüchel, I., A. Güntner, and T. Blume (2016), Use of cosmic-ray neutron sensors for soil moisture monitoring in forests, *Hydrol. Earth Syst. Sci.*, *20*(3), 1269–1288, doi:10.5194/hess-20-1269-2016.

Henn, B., M. P. Clark, D. Kavetski, B. McGurk, T. H. Painter, and J. D. Lundquist (2016), Combining snow, streamflow, and precipitation gauge observations to infer basin-mean precipitation, *Water Resour. Res.*, *52*, 8700–8723, doi:10.1002/2015WR018564.

Jagt, B., A. Lucieer, L. Wallace, D. Turner, and M. Durand (2015), Snow Depth Retrieval with UAS Using Photogrammetric Techniques, *Geosciences*, *5*(3), 264–285, doi:10.3390/geosciences5030264.

Johnson, J. B., and D. Marks (2004), The detection and correction of snow water equivalent pressure sensor errors, *Hydrol. Processes*, *18*(18), 3513–3525, doi:10.1002/hyp.5795.

Jonas, T., C. Marty, and J. Magnusson (2009), Estimating the snow water equivalent from snow depth measurements in the Swiss Alps, *J. Hydrol.*, *378*(1–2), 161–167, doi:10.1016/j.jhydrol.2009.09.021.

Kinar, N. J., and J. W. Pomeroy (2007), Determining snow water equivalent by acoustic sounding, *Hydrol. Processes*, *21*(19), 2623–2640, doi:10.1002/hyp.6793.

Kinar, N. J., and J. W. Pomeroy (2015), Measurement of the physical properties of the snowpack, *Rev. Geophys.*, *53*, 481–544, doi:10.1002/2015RG000481.

Kirnbauer, R., G. Blöschl, and D. Gutknecht (1994), Entering the era of distributed snow models, *Nord. Hydrol.*, *25*, 1–24, doi:10.2166/nh.1994.001.

Kling, H., M. Fuchs, and M. Paulin (2012), Runoff conditions in the upper Danube basin under an ensemble of climate change scenarios, *J. Hydrol.*, *424 425–*, 264–277, doi:10.1016/j.jhydrol.2012.01.011.

Koch, F., M. Prasch, L. Schmid, J. Schweizer, and W. Mauser (2014), Measuring Snow Liquid Water Content with Low-Cost GPS Receivers, *Sensors*, *14*(11), 20,975–20,999, doi:10.3390/s141120975.
Kodama, M. (1980), Continuous monitoring of snow water equivalent using cosmic ray neutrons, *Cold Reg. Sci. Technol.*, *3*(4), 295–303.
Kodama, M. (1984), An introduction to applied cosmic ray physics, *Jpn. J. Appl. Phys.*, *23*(6R), 726–728, doi:10.1143/JJAP.23.726.
Köhli, M., M. Schrön, M. Zreda, U. Schmidt, P. Dietrich, and S. Zacharias (2015), Footprint characteristics revised for field-scale soil moisture monitoring with cosmic-ray neutrons, *Water Resour. Res.*, *51*, 5772–5790, doi:10.1002/2015WR017169.
Liang, T., X. Zhang, H. Xie, C. Wu, Q. Feng, X. Huang, and Q. Chen (2008), Toward improved daily snow cover mapping with advanced combination of MODIS and AMSR-E measurements, *Remote Sens. Environ.*, *112*(10), 3750–3761, doi:10.1016/j.rse.2008.05.010.
Liniger, H., R. Weingartner, and M. Grosjean (1998), *Mountains of the World: Water Towers for the 21st Century*, Dep. of Geogr., Univ. of Berne, Berne, Switzerland.
López-Moreno, J. I., S. R. Fassnacht, J. T. Heath, K. N. Musselman, J. Revuelto, J. Latron, E. Morán-Tejeda, and T. Jonas (2013), Small scale spatial variability of snow density and depth over complex alpine terrain: Implications for estimating snow water equivalent, *Adv. Water Resour.*, *55*, 40–52, doi:10.1016/j.advwatres.2012.08.010.
Lundberg, A., N. Granlund, and D. Gustafsson (2010), Towards automated ''Ground truth'' snow measurements—a review of operational and new measurement methods for Sweden, Norway, and Finland, *Hydrol. Processes*, *24*(14), 1955–1970, doi:10.1002/hyp.7658.
Lundberg, A., D. Gustafsson, C. Stumpp, B. Kløve, and J. Feiccabrino (2016), Spatiotemporal variations in snow and soil frost: A review of measurement techniques, *Hydrology*, *3*(3), 28, doi:10.3390/hydrology3030028.
Magnusson, J., D. Gustafsson, F. Hüsler, and T. Jonas (2014), Assimilation of point SWE data into a distributed snow cover model comparing two contrasting methods, *Water*, *50*, 7816–7835, doi:10.1002/2014WR015302.
Marchand, W.-D., and Å. Killingtveit (2005), Statistical probability distribution of snow depth at the model sub-grid cell spatial scale, *Hydrol. Processes*, *19*(2), 355–369, doi:10.1002/hyp.5543.
Morris, E. M. (2008), A theoretical analysis of the neutron scattering method of measuring snow and ice density, *J. Geophys. Res.*, *113*, F03019, doi:10.1029/2007JF000962.
Nagler, T., H. Rott, E. Ripper, G. Bippus, and M. Hetzenecker (2016), Advancements for Snowmelt Monitoring by Means of Sentinel-1 SAR, *Remote Sens.*, *8*(4), 348, doi:10.3390/rs8040348.
Nolan, M., C. Larsen, and M. Sturm (2015), Mapping snow depth from manned aircraft on landscape scales at centimeter resolution using structure-from-motion photogrammetry, *Cryosphere*, *9*(4), 1445–1463, doi:10.5194/tc-9-1445-2015.
Nolin, A. W. (2010), Recent advances in remote sensing of seasonal snow, *J. Glaciol.*, *56*(200), 1141–1150, doi:10.3189/002214311796406077.
Paquet, E., and M.-T. Laval (2006), Retour d'expérience et perspectives d'exploitation des Nivomètres à Rayonnement Cosmique d'EDF, *La Houille Blanche*, (2), 113–119, doi:10.1051/lhb:200602015.
Peck, E. L., V. C. Bissell, E. B. Jones, and D. L. Burge (1971), Evaluation of Snow Water Equivalent by Airborne Measurement of Passive Terrestrial Gamma Radiation, *Water Resour. Res.*, *7*(5), 1151–1159, doi:10.1029/WR007i005p01151.
Pettinato, S., E. Santi, M. Brogioni, S. Paloscia, E. Palchetti, and C. Xiong (2013), The potential of COSMO-SkyMed SAR images in monitoring snow cover characteristics, *IEEE Geosci. Remote Sens. Lett.*, *10*(1), 9–13, doi:10.1109/LGRS.2012.2189752.
Proksch, M., N. Rutter, C. Fierz, and M. Schneebeli (2016), Intercomparison of snow density measurements: Bias, precision, and vertical resolution, *Cryosphere*, *10*(1), 371–384, doi:10.5194/tc-10-371-2016.
Rasmussen, R., et al. (2012), How well are we measuring snow: The NOAA/FAA/NCAR winter precipitation test bed, *Bull. Am. Meteorol. Soc.*, *93*(6), 811–829, doi:10.1175/BAMS-D-11-00052.1.
Revuelto, J., V. Vionnet, J.-I. López-Moreno, M. Lafaysse, and S. Morin (2016), Combining snowpack modeling and terrestrial laser scanner observations improves the simulation of small scale snow dynamics, *J. Hydrol.*, *533*, 291–307, doi:10.1016/j.jhydrol.2015.12.015.
Rittger, K., T. H. Painter, and J. Dozier (2013), Assessment of methods for mapping snow cover from MODIS, *Adv. Water Resour.*, *51*, 367–380, doi:10.1016/j.advwatres.2012.03.002.
Rivera Villarreyes, C. A., G. Baroni, and S. E. Oswald (2011), Integral quantification of seasonal soil moisture changes in farmland by cosmic-ray neutrons, *Hydrol. Earth Syst. Sci.*, *15*(12), 3843–3859, doi:10.5194/hess-15-3843-2011.
Rivera Villarreyes, C. A., G. Baroni, and S. E. Oswald (2014), Inverse modeling of cosmic-ray soil moisture for field-scale soil hydraulic parameters, *Eur. J. Soil Sci.*, *65*(6), 876–886, doi:10.1111/ejss.12162.
Rondeau-Genesse, G., M. Trudel, and R. Leconte (2016), Monitoring snow wetness in an Alpine Basin using combined C-band SAR and MODIS data, *Remote Sens. Environ.*, *183*, 304–317, doi:10.1016/j.rse.2016.06.003.
Rosolem, R. et al. (2013), The effect of atmospheric water vapor on neutron count in the cosmic-ray soil moisture observing system, *J. Hydrometeorol.*, *14*, 1659–1671. [Available at https://doi.org/10.1175/JHM-D-12-0120.1.]
Rott, H., T. Nagler, and R. Scheiber (2004), Snow mass retrieval by means of SAR interferometry, in *Proceedings of FRINGE 2003 Workshop, Frascati, Italy, 1–5 December 2003*, pp. 187–192, Eur. Space Agency, (Special Publication) ESA SP. [Available at http://earth.esa.int/workshops/fringe03/proceedings/papers/46_rott.pdf.]
Rott, H., et al. (2012), Algorithm for retrieval of snow mass from Ku- and X-band radar backscatter measurements, in *International Geoscience and Remote Sensing Symposium (IGARSS)*, pp. 135–138, IEEE, New York. [Available at https://doi.org/10.1109/IGARSS.2012.6350911.]
Schöber, J., K. Schneider, K. Helfricht, P. Schattan, S. Achleitner, F. Schöberl, and R. Kirnbauer (2014), Snow cover characteristics in a glacierized catchment in the Tyrolean Alps: Improved spatially distributed modelling by usage of Lidar data, *J. Hydrol.*, *519*, 3492–3510, doi:10.1016/j.jhydrol.2013.12.054.
Schöber, J., S. Achleitner, J. Bellinger, R. Kirnbauer, and F. Schöberl (2016), Analysis and modelling of snow bulk density in the Tyrolean alps, *Hydrol. Res.*, *47*(2), 417–441, doi:10.2166/nh.2015.132.
Shrestha, M., L. Wang, T. Koike, H. Tsutsui, Y. Xue, and Y. Hirabayashi (2014), Correcting basin-scale snowfall in a mountainous basin using a distributed snowmelt model and remote-sensing data, *Hydrol. Earth Syst. Sci.*, *18*(2), 747–761, doi:10.5194/hess-18-747-2014.
Shuttleworth, J., R. Rosolem, M. Zreda, and T. Franz (2013), The COsmic-ray Soil Moisture Interaction Code (COSMIC) for use in data assimilation, *Hydrol. Earth Syst. Sci.*, *17*(8), 3205–3217, doi:10.5194/hess-17-3205-2013.
Sigouin, M. J. P., and B. C. Si (2016), Calibration of a non-invasive cosmic-ray probe for wide area snow water equivalent measurement, *Cryosphere*, *10*(3), 1181–1190, doi:10.5194/tc-10-1181-2016.
Slater, A. G., and M. P. Clark (2006), Snow data assimilation via an ensemble Kalman filter, *J. Hydrometeorol.*, *7*(3), 478–493, doi:10.1175/JHM505.1.
Stähli, M., M. Stacheder, D. Gustafsson, S. Schlaeger, M. Schneebeli, and A. Brandelik (2004), A new in situ sensor for large-scale snow-cover monitoring, *Ann. Glaciol.*, *38*(1), 273–278, doi:10.3189/172756404781814933.
Stuefer, S., D. L. Kane, and G. E. Liston (2013), *In situ* snow water equivalent observations in the US Arctic, *Hydrol. Res.*, *44*(1), 21–34, doi:10.2166/nh.2012.177.

Sturm, M. (2015), White water: Fifty years of snow research in WRR and the outlook for the future, *Water Resour. Res.*, *51*, 4948–4965, doi: 10.1002/2015WR017242.Received.

Sturm, M., J. Holmgren, and G. E. Liston (1995), A seasonal snow cover classification system for local to global applications, *J. Clim.*, *8*(5), 1261–1283, doi:10.1175/1520-0442(1995)008<;1261:ASSCCS>;2.0.CO;2.

Sturm, M., B. Taras, G. E. Liston, C. Derksen, T. Jonas, and J. Lea (2010), Estimating snow water equivalent using snow depth data and climate classes, *J. Hydrometeorol.*, *11*(6), 1380–1394, doi:10.1175/2010JHM1202.1.

Thirel, G., P. Salamon, P. Burek, and M. Kalas (2013), Assimilation of MODIS snow cover area data in a distributed hydrological model using the particle filter, *Remote Sens.*, *5*, 5825–5850, doi:10.3390/rs5115825.

Tian, Z., Z. Li, G. Liu, B. Li, and T. Ren (2016), Soil water content determination with cosmic-ray neutron sensor: Correcting aboveground hydrogen effects with thermal/fast neutron ratio, *J. Hydrol.*, *540*, 923–933, doi:10.1016/j.jhydrol.2016.07.004.

Viviroli, D., H. H. Dürr, B. Messerli, M. Meybeck, and R. Weingartner (2007), Mountains of the world, water towers for humanity: Typology, mapping, and global significance, *Water Resour. Res.*, *43*, W07447, doi:10.1029/2006WR005653.

Zreda, M., D. Desilets, T. P. A. Ferré, and R. L. Scott (2008), Measuring soil moisture content non-invasively at intermediate spatial scale using cosmic-ray neutrons, *Geophys. Res. Lett.*, *35*, L21402, doi:10.1029/2008GL035655.

Zreda, M., W. J. Shuttleworth, X. Zeng, C. Zweck, D. Desilets, T. Franz, and R. Rosolem (2012), COSMOS: the COsmic-ray Soil Moisture Observing System, *Hydrol. Earth Syst. Sci.*, *16*(11), 4079–4099, doi:10.5194/hess-16-4079-2012.

Zweck, C., M. Zreda, and D. Desilets (2013), Snow shielding factors for cosmogenic nuclide dating inferred from Monte Carlo neutron transport simulations, *Earth Planet. Sci. Lett.*, *379*, 64–71, doi:10.1016/j.epsl.2013.07.023.